Supporting Information

Record-high Power Output in Flexible Gelatin/GTA-KCl-$FeCN^{4-/3-}$ Ionic Thermoelectric Cells Enable by Enlarging Working Temperature Range

*Yuchen Li, Qikai Li, Xinbo Zhang, Jiajia Zhang, Shuaihua Wang, Liuqin Lai, Kang Zhu, Weishu Liu**

Yuchen Li, Qikai Li, Xinbo Zhang, Jiajia Zhang, Shuaihua Wang, Liuqin Lai, Kang Zhu, Weishu Liu

Department of Materials Science and Engineering, Southern University of Science and Technology, Shenzhen, Guangdong 518055, China

Email: liuws@sustech.edu.cn

Weishu Liu

Shenzhen Engineering Research Center for Novel Electronic Information Materials and Devices, Southern University of Science and Technology, Shenzhen, Guangdong 518055, China

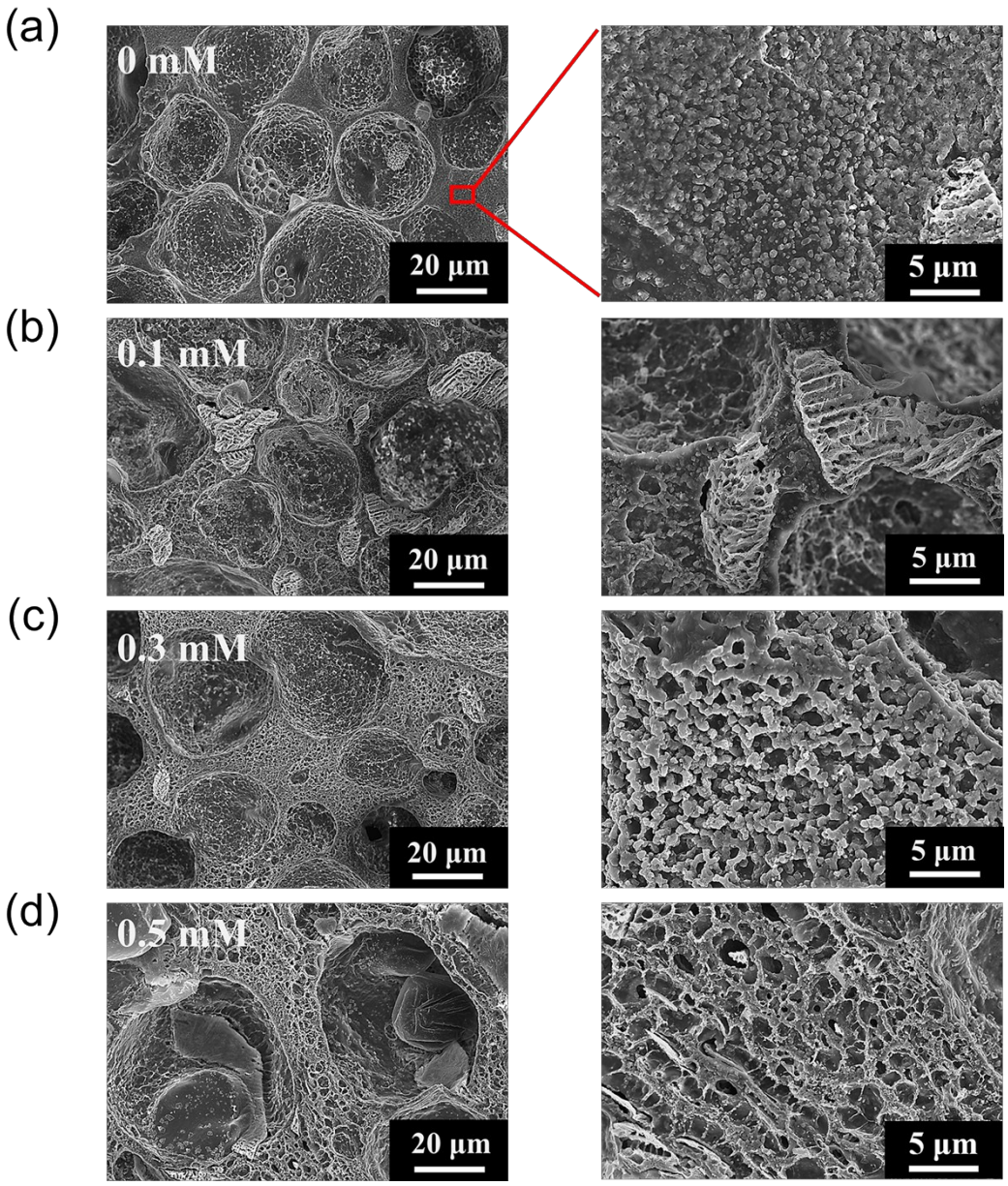

Figure S1. SEM images of the freeze-dried Gelatin/x GTA-KCl-$FeCN^{4-/3-}$ i-TE gels (r_v = 3.0) a) x = 0 mM. b) x = 0.1 mM. c) x = 0.3 mM. d) x = 0.5 mM.

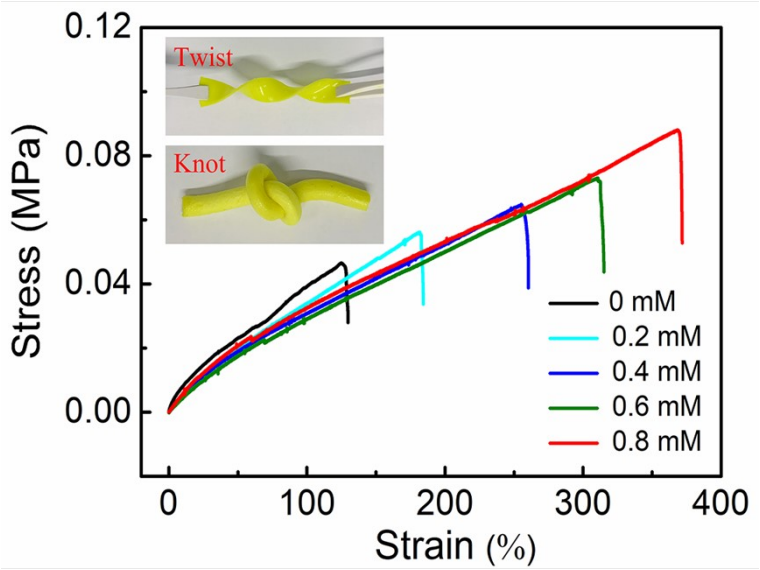

Figure S2. Tensile stress-strain curves for Gelatin/ x GTA-KCl-$FeCN^{4-/3-}$ (x = 0, 0.2, 0.4, 0.6 and 0.8 mM, r_v = 3.0).

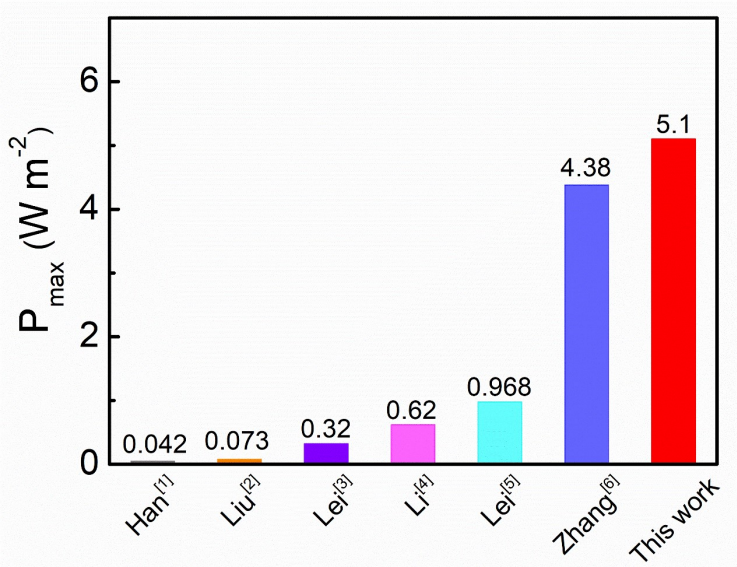

Figure S3. Comparison of the P_{max} of Gelatin/0.8 mM GTA-KCl-$FeCN^{4-/3-}$ (r_v = 2.8) with that of the reported quasi-solid-state i-TE cells.

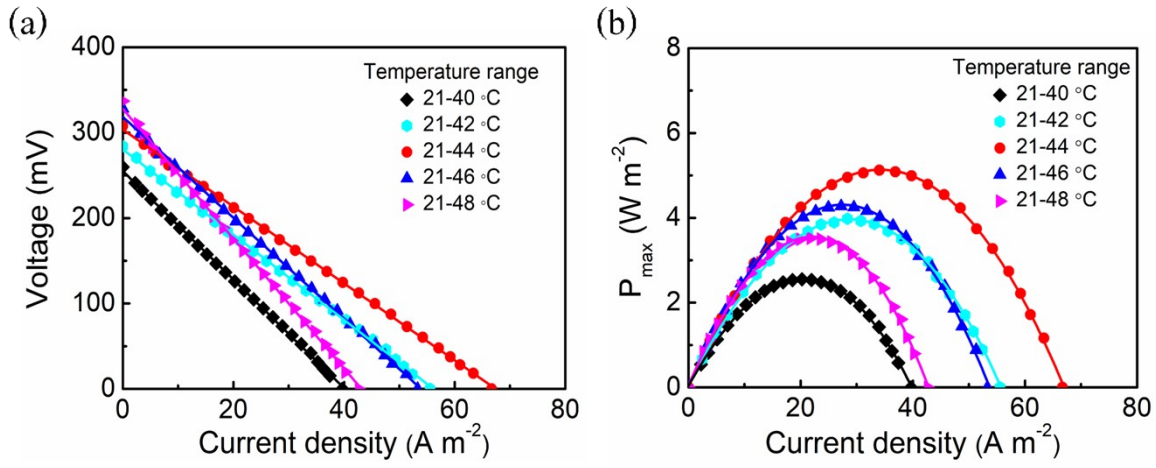

Figure S4. a) Voltage and b) output power density versus current density for the optimal sample Au/Cu | Gelatin/0.8 mM GTA-KCl-$FeCN^{4-/3-}$ (r_v = 2.8) | Au/Cu i-TE cell under different T_H (T_H = 40, 42, 44, 46, and 48 °C) with a fixed T_C = 21 °C.

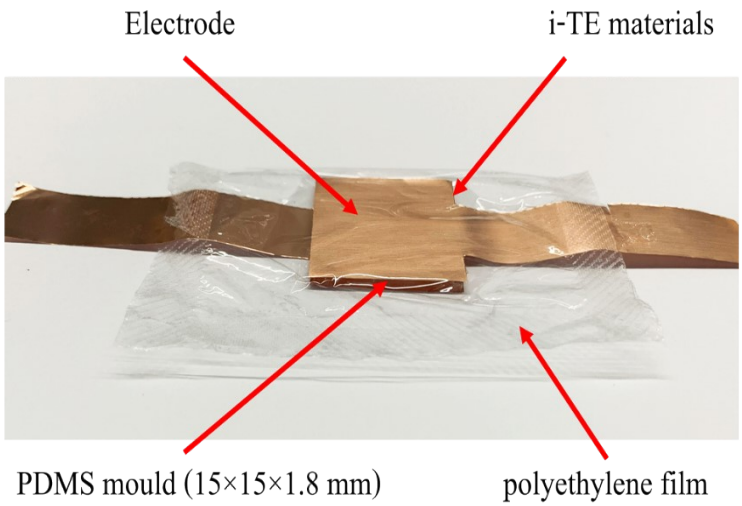

Figure S5. The as-fabricated i-TE cell is assembled as Au/Cu | i-TE | Au/Cu structure with a PDMS mold. The dimension of the i-TE cell is 15 × 15 × 1.8 mm. The i-TE material is Gelatin/*x* GTA-0.8 M KCl-0.42/0.25 M $FeCN^{4-/3-}$. The concentrations of KCl and GTA are fixed at 0.8 M and 0.42/0.25 M, according to the optimal concentration in our previous work.[1] The *x* and the volume ratio of water to gelatin (r_v) are adjusted in this work.

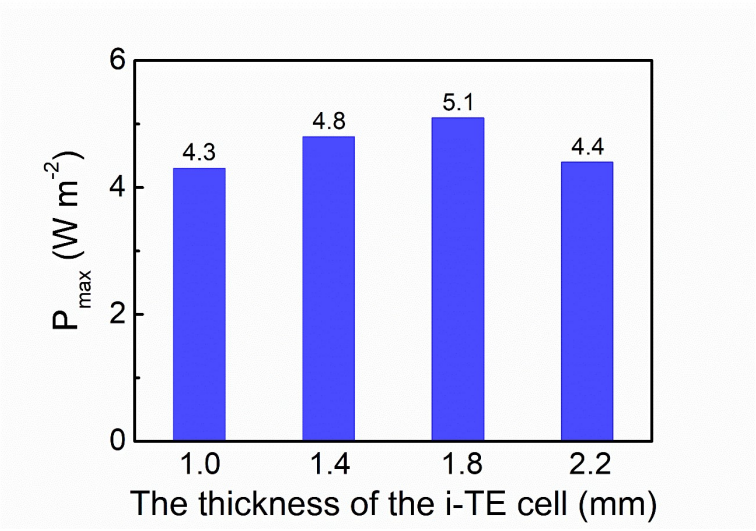

Figure S6. The output power density of the Au/Cu | Gelatin/0.8 mM GTA-KCl-$FeCN^{4-/3-}$ (r_v = 2.8) | Au/Cu i-TE cells with different thicknesses.

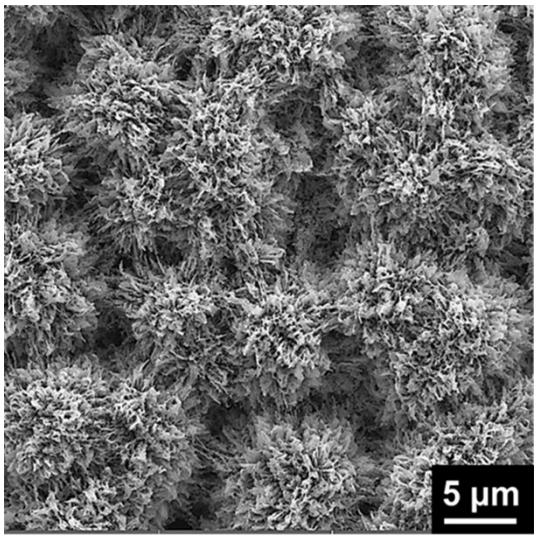

Figure S7. SEM image of the 3D microflower Au/Cu electrode

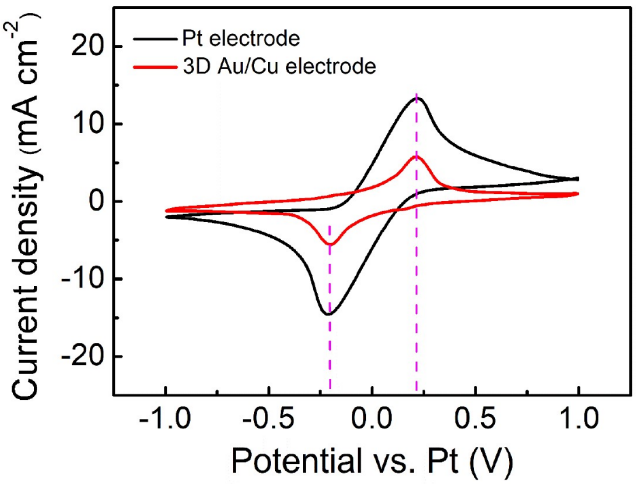

Figure S8. Cyclic voltammetry (CV) curves of Au/Cu | Gelatin-KCl-$FeCN^{4-/3-}$ (r_v = 3) | Au/Cu and Pt | Gelatin-KCl-$FeCN^{4-/3-}$ | Pt i-TE cells at a rate of 50 mV K^{-1}. The scanning voltage range is from -1.0 V to +1.0 V. The anodic and cathodic peaks near 0.2 V and -0.2 V is the redox reaction peaks of $FeCN^{4-/3-}$. The detailed study of Au/Cu electrodes has been illuminated in our previously reported work.[6]

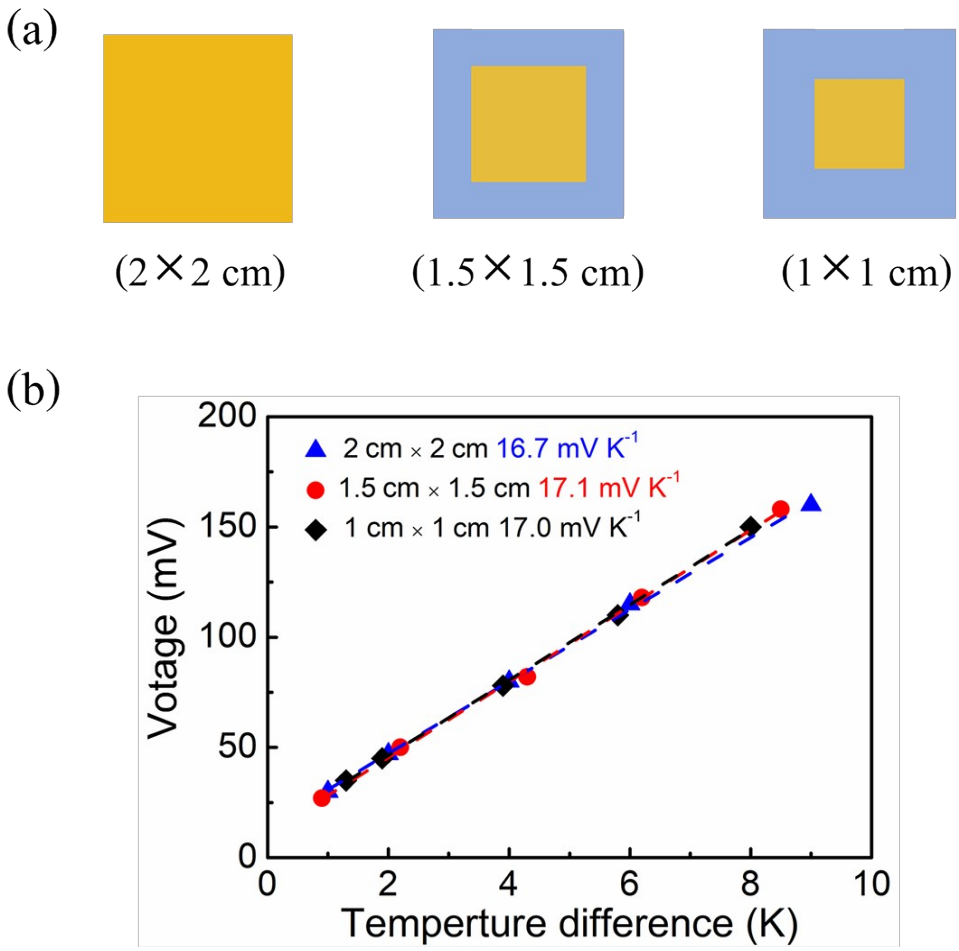

Figure S9. The effect of the Au/Cu electrodes on the thermopower of Au/Cu | Gelatin-KCl-$FeCN^{4-/3-}$ ($r_v = 3$) | Au/Cu. a) Three different sizes of the Au/Cu electrodes. b) The thermopower measurement of Au/Cu electrodes with different sizes. The Au/Cu electrodes with different sizes show a comparable thermopower near 17 mV K^{-1}. The results are corresponding to our previous work, indicating that the Au/Cu electrodes have no significant effect on the thermopower.

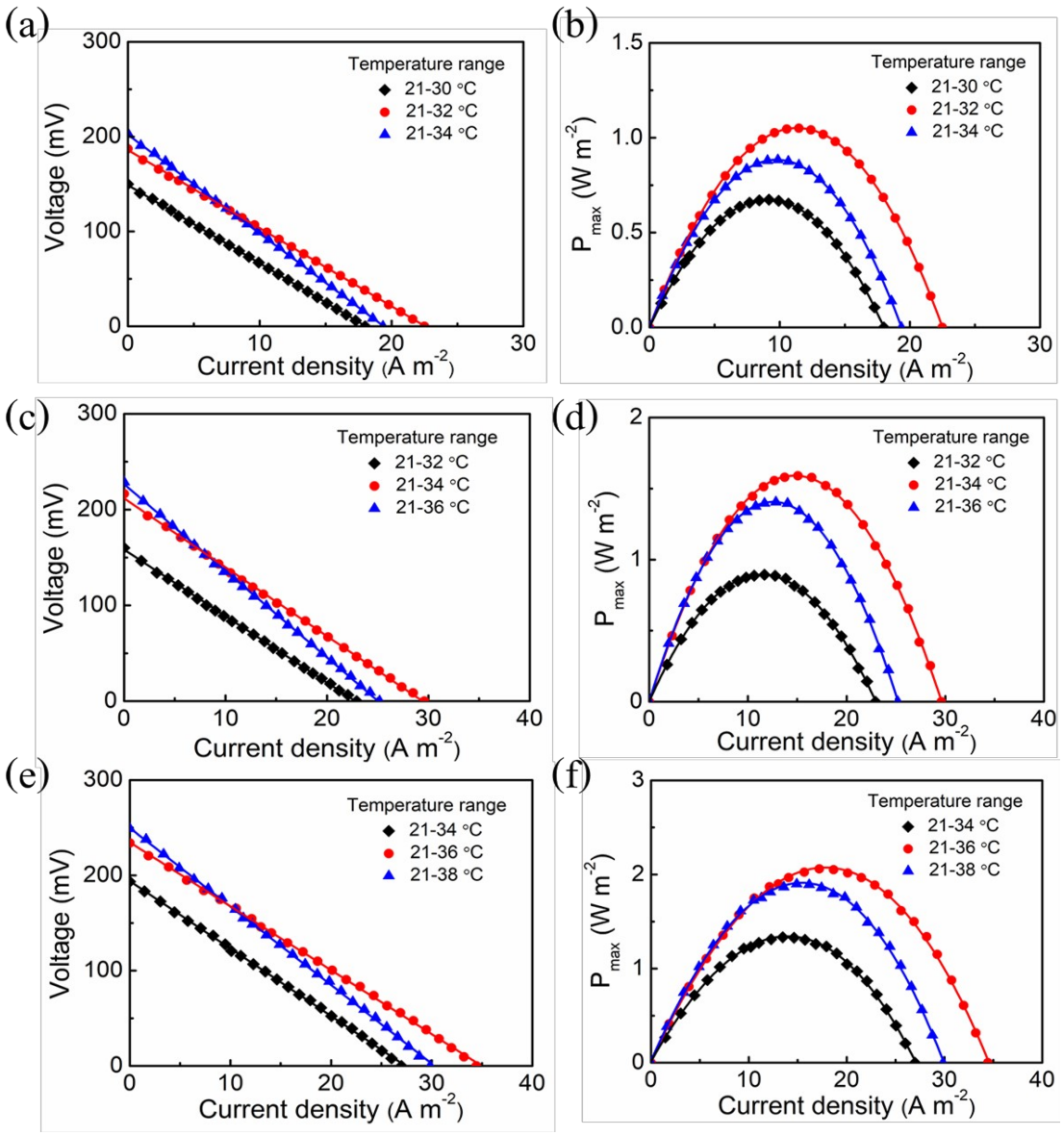

Figure S10. Voltage and output power density versus current density for the as-fabricated Au/Cu | Gelatin/x GTA-KCl-$FeCN^{4-/3-}$ ($r_v = 3$) | Au/Cu i-TE cell under different T_H with a fixed $T_C = 21$ °C. a) and b) $x = 0.4$ mM, $T_H = 30$, 32, and 34 °C. c) and d) $x = 0.5$ mM, $T_H = 32$, 34, and 36 °C. e) and f) $x = 0.6$ mM, $T_H = 34$, 36, and 38 °C. The T_C is set at 21 °C according to the suggested temperature in our previous work,[6] because the lower T_C results in higher internal resistance and lower P_{max}.[6,7]

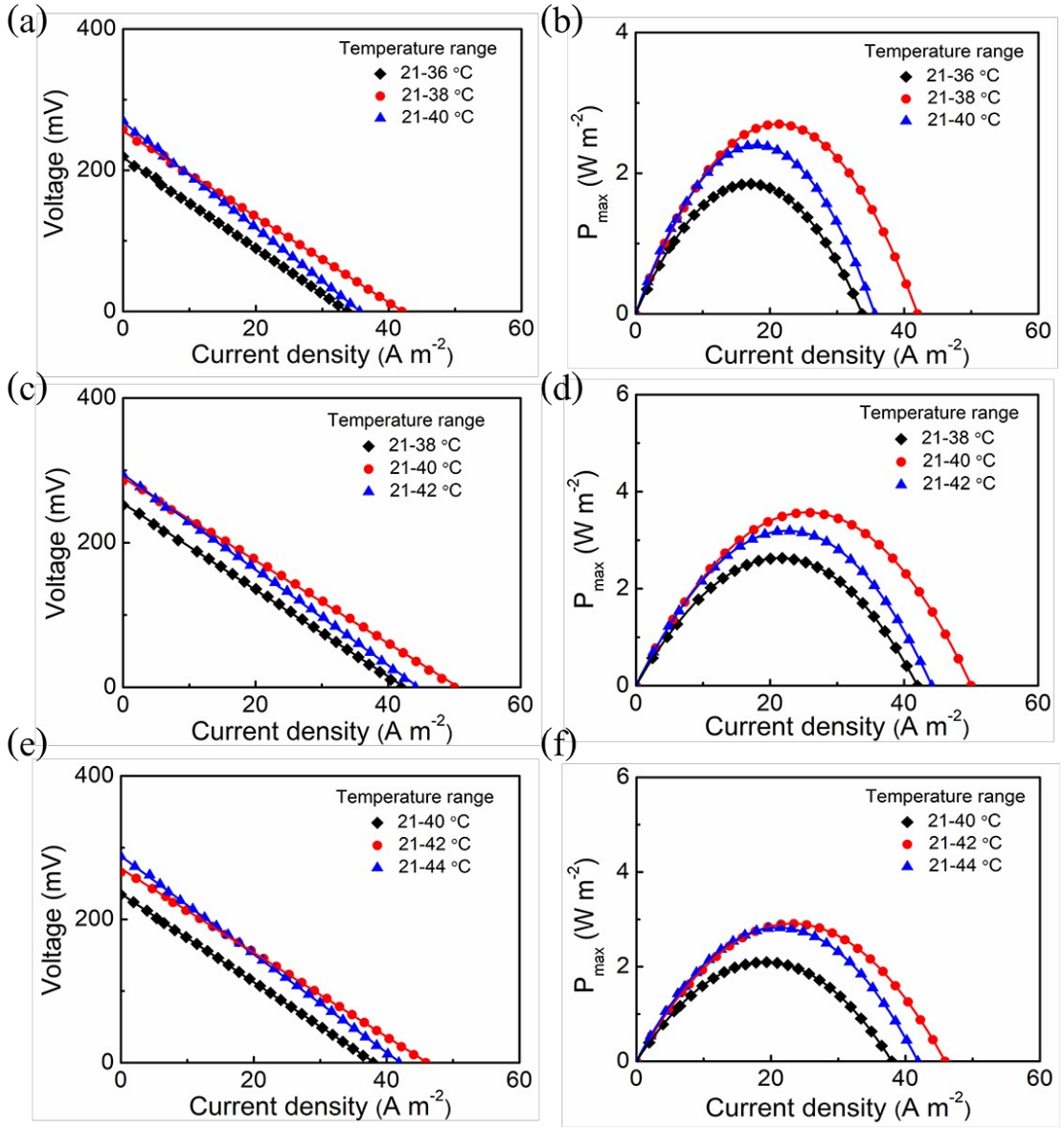

Figure S11. Voltage and output power density versus current density for the as-fabricated Au/Cu | Gelatin/x GTA-KCl-$FeCN^{4-/3-}$ ($r_v = 3$) | Au/Cu i-TE cell under different T_H with a fixed $T_C = 21$ °C. a) and b) $x = 0.7$ mM, $T_H = 36$, 38, and 40 °C. c) and d) $x = 0.8$ mM, $T_H = 38$, 40, and 42 °C. e) and f) $x = 0.9$ mM, $T_H = 40$, 42, and 44 °C.

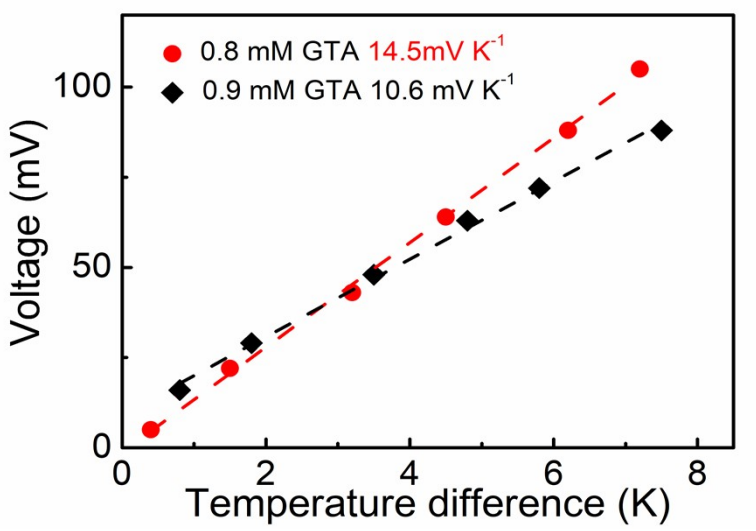

Figure S12. Thermopower measurement of the Au/Cu | Gelatin/0.8 mM GTA-KCl-$FeCN^{4-/3-}$ (r_v = 3) | Au/Cu and Au/Cu | Gelatin/0.9 mM GTA-KCl-$FeCN^{4-/3-}$ (r_v = 3) | Au/Cu i-TE cells.

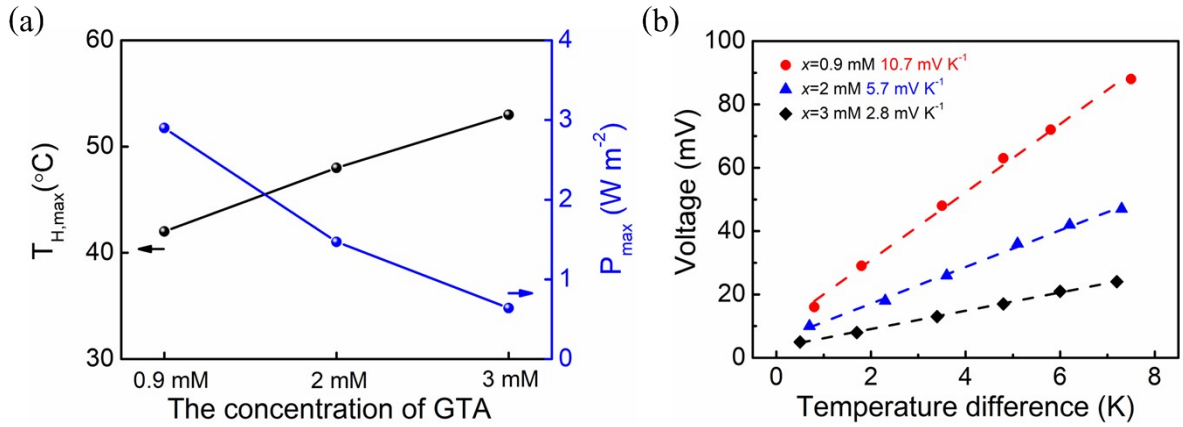

Figure S13. a) The $T_{H,max}$ and P_{max} of the Au/Cu | Gelatin/x mM GTA-KCl-FeCN$^{4-/3-}$ (r_v = 3) | Au/Cu, x =0.9, 2, and 3 mM. b) Thermopower measurement of the Au/Cu | Gelatin/ x mM GTA-KCl-FeCN$^{4-/3-}$ (r_v = 3) | Au/Cu i-TE cells, x =0.9, 2, and 3 mM.

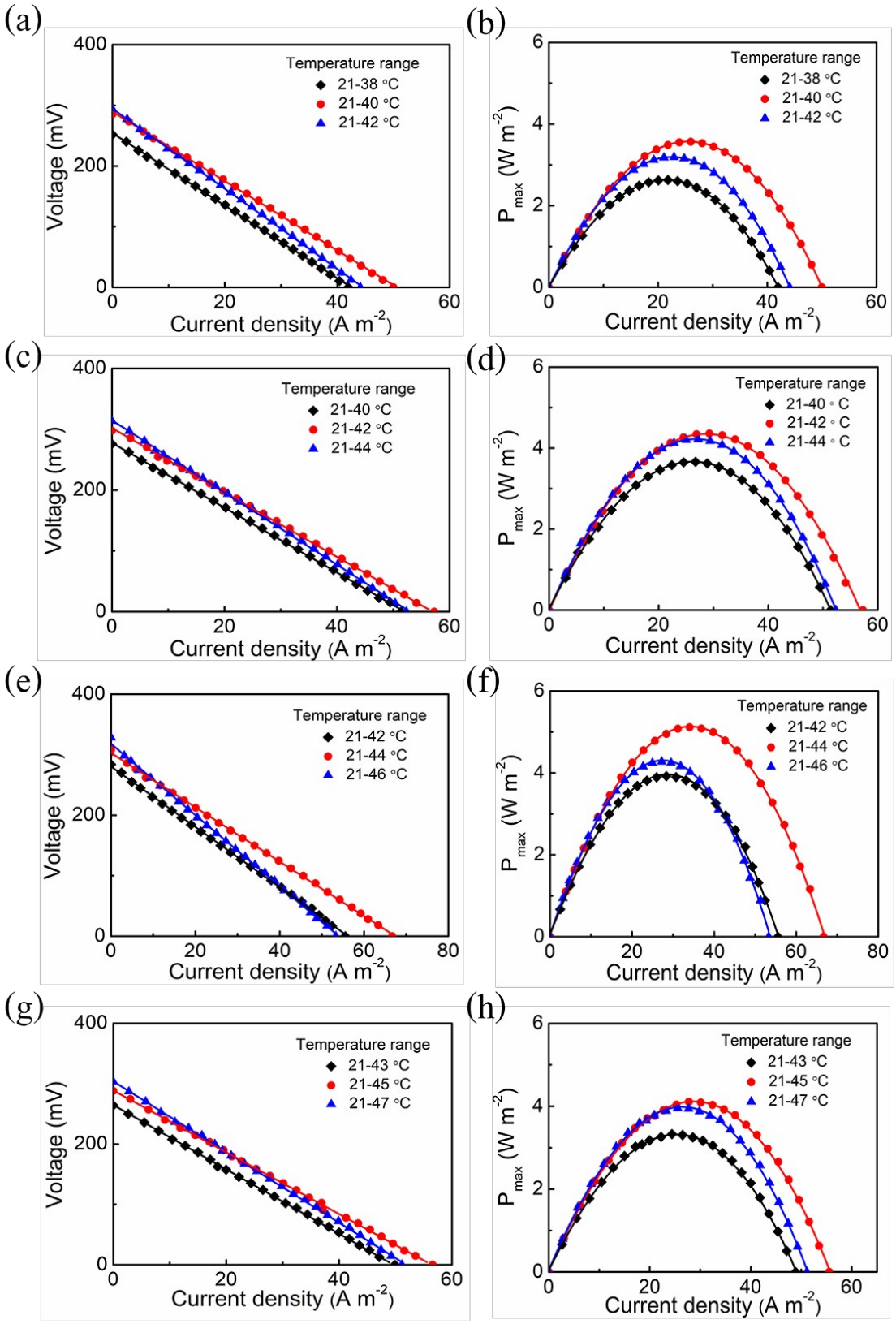

Figure S14. Voltage and output power density versus current density for the as-fabricated Au/Cu | Gelatin/0.8 mM GTA-KCl-$FeCN^{4-/3-}$ (at different r_v) | Au/Cu i-TE cell under different T_H with a fixed T_C = 21 °C. a) and b) r_v = 3, T_H = 38, 40, and 42 °C. c) and d) r_v = 2.9, T_H =

40, 42, and 44 ℃. e) and f) r_v = 2.8, T_H = 42, 44, and 46 ℃. g) and h) r_v = 2.7, T_H = 43, 45, and 47 ℃.

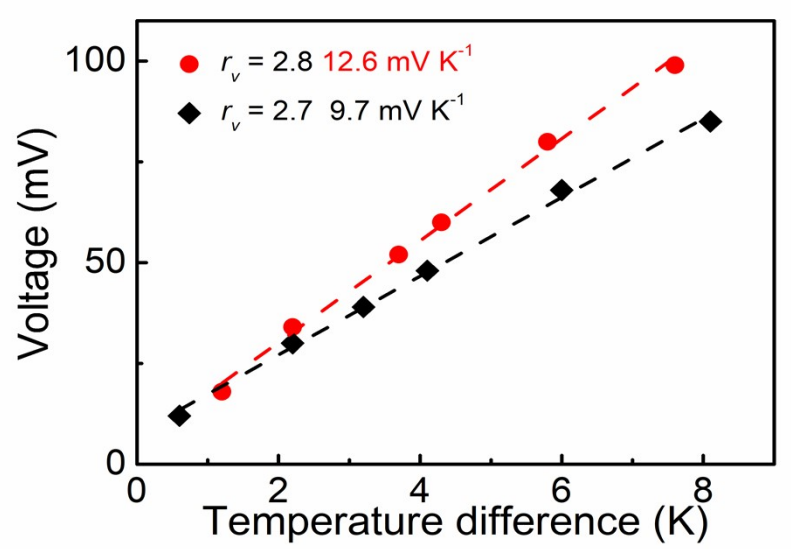

Figure S15. Thermopower measurement of the as-fabricated Au/Cu | Gelatin/0.8 mM GTA-KCl-$FeCN^{4-/3-}$ (r_v = 2.8) | Au/Cu and Au/Cu | Gelatin/0.8 mM GTA-KCl-$FeCN^{4-/3-}$ (r_v = 2.7)| Au/Cu i-TE cells.

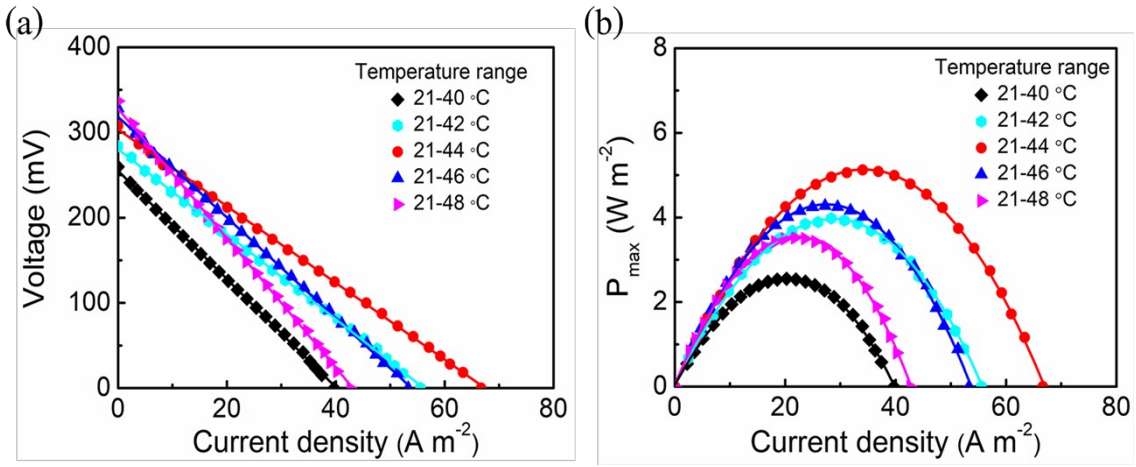

Figure S16. a) Voltage and b) output power density versus current density for the optimal sample Au/Cu | Gelatin/0.8 mM GTA-KCl-$FeCN^{4-/3-}$ ($r_v = 2.8$) | Au/Cu i-TE cell under different T_H (40, 42, 44, 46, and 48 °C) with a fixed $T_C = 21$ °C.

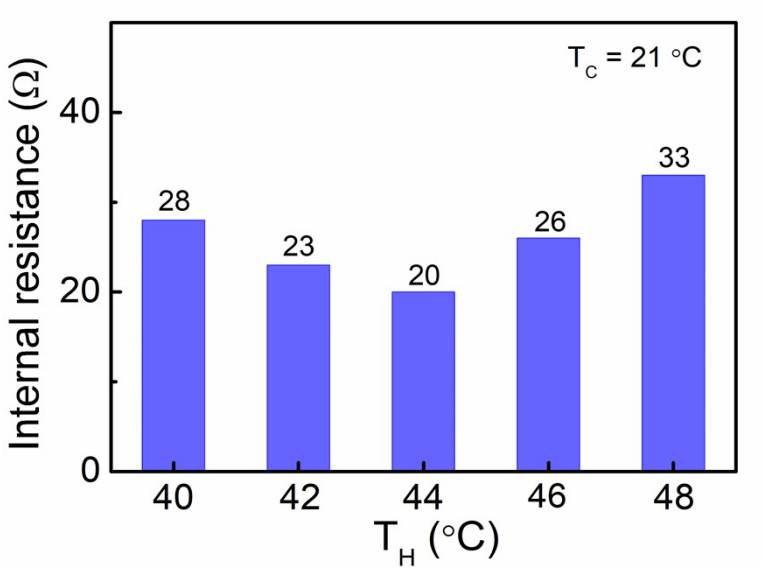

Figure S17. The internal resistance for the as-fabricated Au/Cu | Gelatin/0.8 mM GTA-KCl-$FeCN^{4-/3-}$ (r_v = 2.8) | Au/Cu i-TE cell under different T_H (40, 42, 44, 46 and 48 °C) with a fixed T_C = 21 °C.

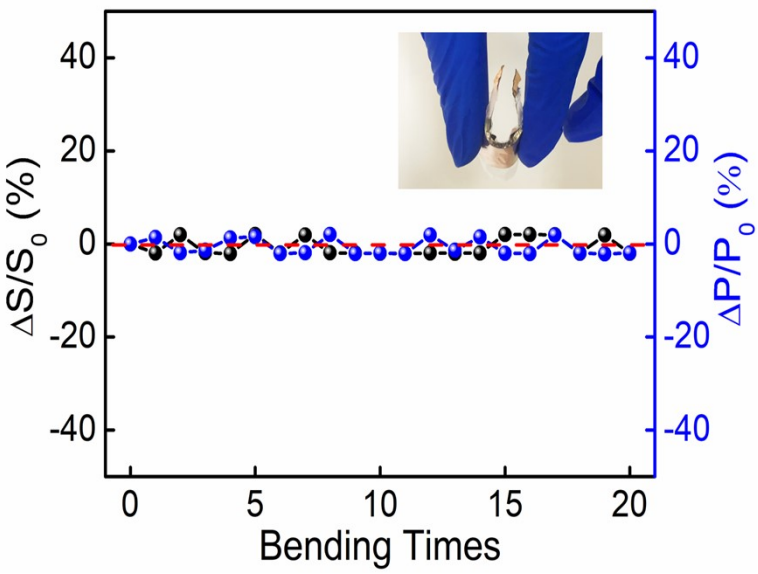

Figure S18. The thermopower and output power fluctuation of the Au/Cu | Gelatin/0.8 mM GTA-KCl-$FeCN^{4-/3-}$ (r_v = 2.8) | Au/Cu i-TE cell after bending 20 times.

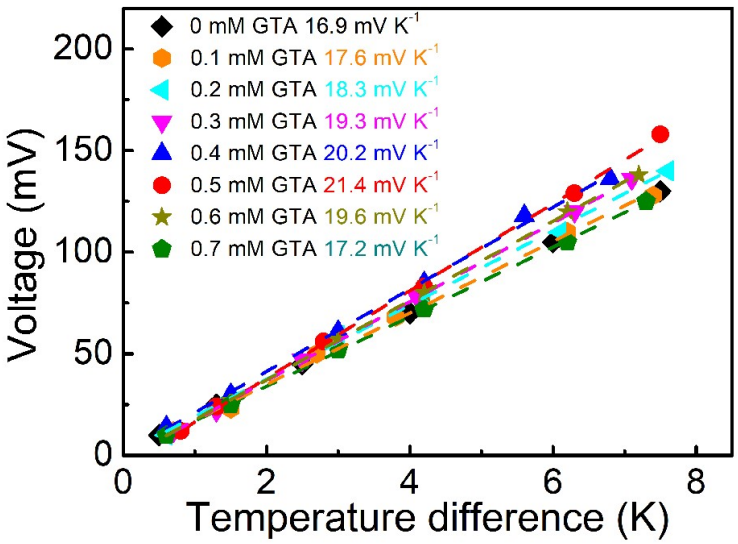

Figure S19. Thermopower measurement of the as-fabricated Au/Cu | Gelatin/x GTA-KCl-$FeCN^{4-/3-}$ (r_v = 3) | Au/Cu i-TE cells (x = 0, 0.1, 0.2, 0.3, 0.4, 0.5, 0.6, and 0.7 mM).

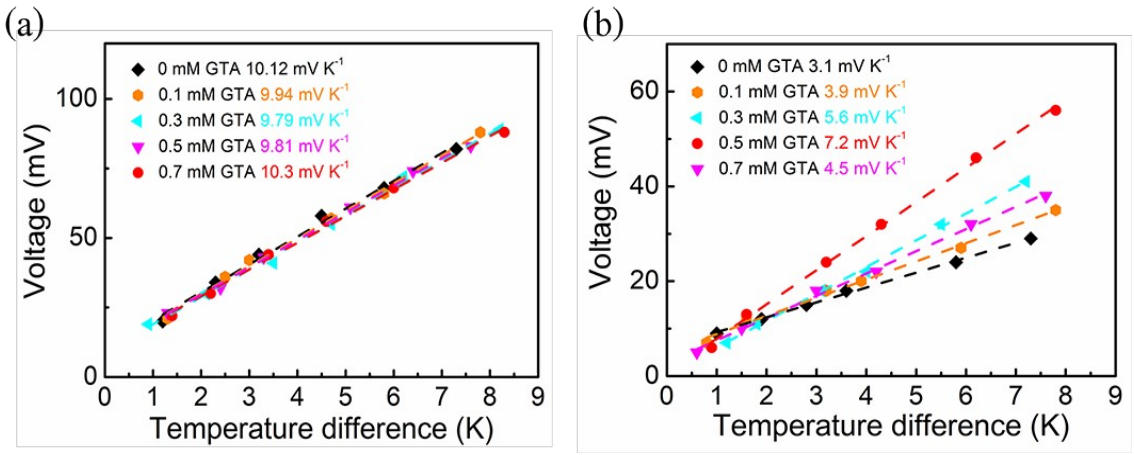

Figure S20. Thermopower measurement of a) the as-fabricated Au/Cu | Gelatin/*x* GTA-0.8 M KCl (r_v = 3) | Au/Cu i-TE cells and b) Au/Cu | Gelatin/*x* GTA-0.42/0.25 M $FeCN^{4-/3-}$ (r_v = 3) | Au/Cu i-TE cells (*x* = 0, 0.1, 0.3, 0.5, and 0.7 mM).

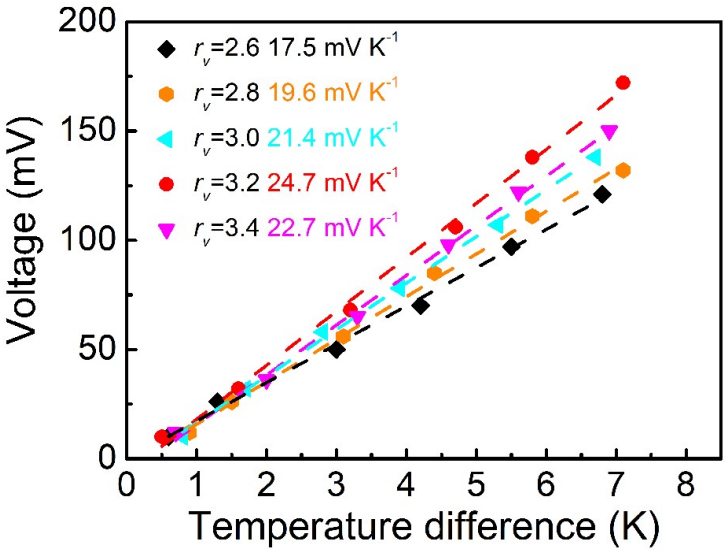

Figure S21. Thermopower measurement of the as-fabricated Au/Cu | Gelatin/0.5 mM GTA-KCl-$FeCN^{4-/3-}$ (r_v =2.6, 2.8, 3.0, 3.2, and 3.4) | Au/Cu i-TE cells.

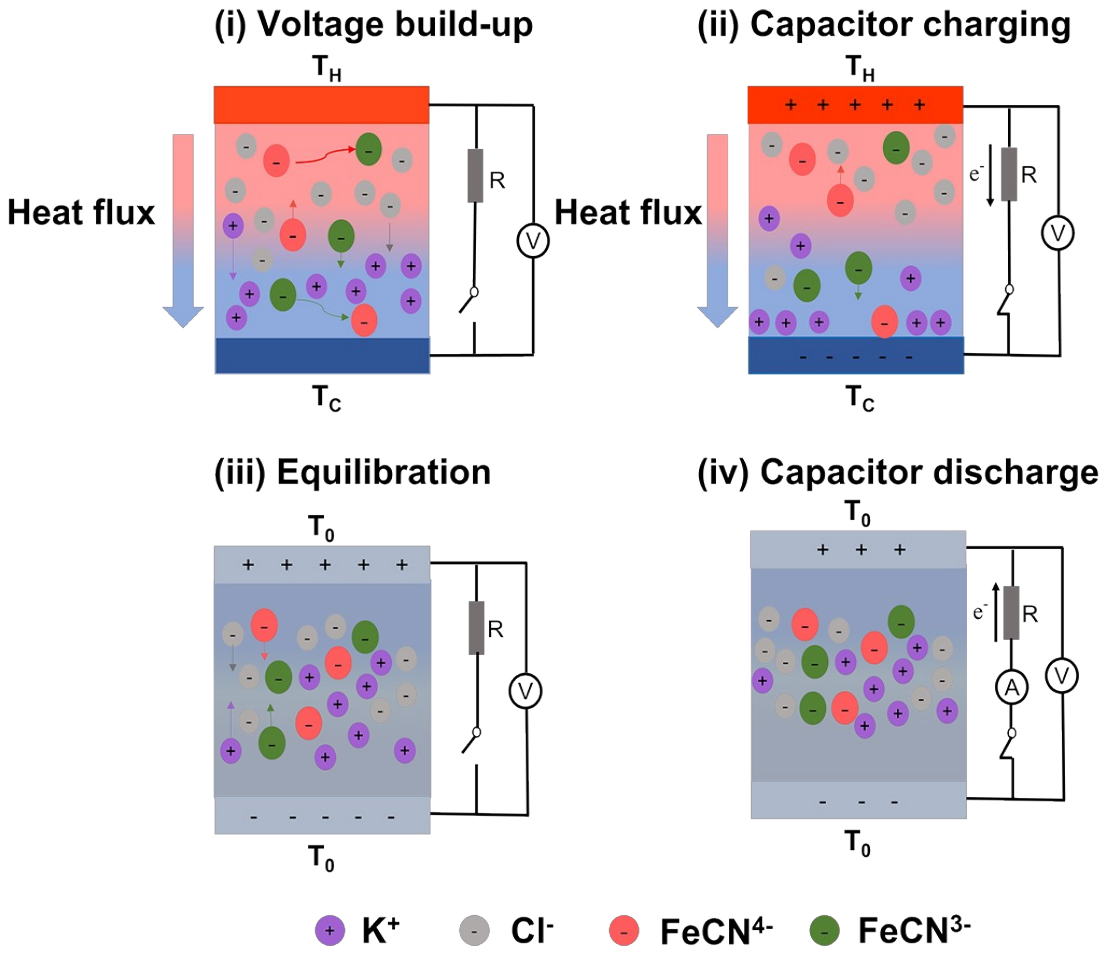

Figure S22. Schematic illustration for the Gelatin-KCl-$FeCN^{4-/3-}$ i-TE capacitor working mode. There are four stages totally: (i) voltage build-up, (ii) capacitor charging, (iii) equilibration, and (iv) capacitor discharge. This mode was adopted by several groups, such as Crispin et al. at Linköping University,[8] Yu et al. at Texas A&M University,[9] and Jang et al. at UNIST.[10]

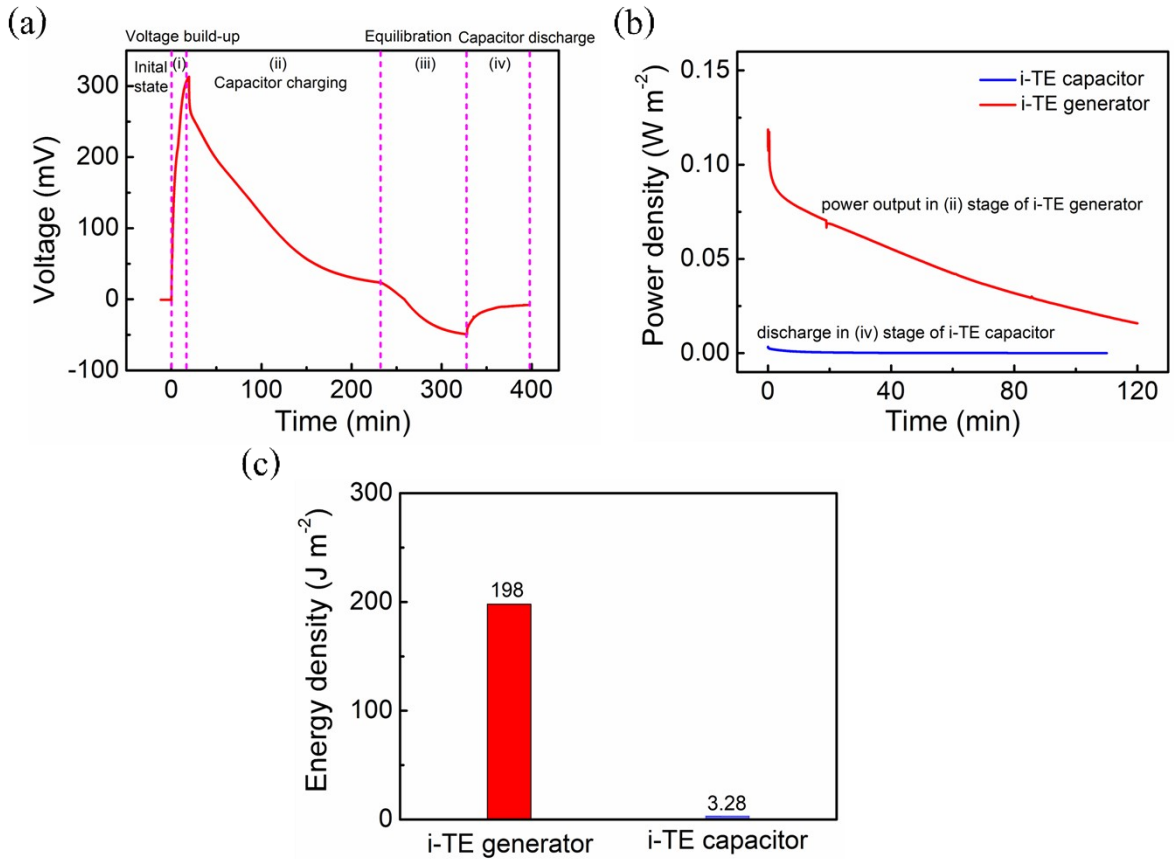

Figure S23. a) The measured voltage curve for the as-fabricated Au/Cu | Gelatin/0.8 mM GTA-KCl-$FeCN^{4-/3-}$ (r_v = 2.8) | Au/Cu i-TE cell at ΔT = 23 K (temperature range: from 21 °C to 44 °C). The load resistance in (ii) and (iv) stages is 3000 Ω. The comparison of b) power density and c) energy density using the i-TE capacitor and i-TE generator modes, respectively. The power density measurement for the i-TE generator is the (ii) stage called power output in Figure 5a and for the i-TE capacitor is the (iv) stage called capacitor discharge in Figure S17. The energy density is the integral of power density over corresponding time.

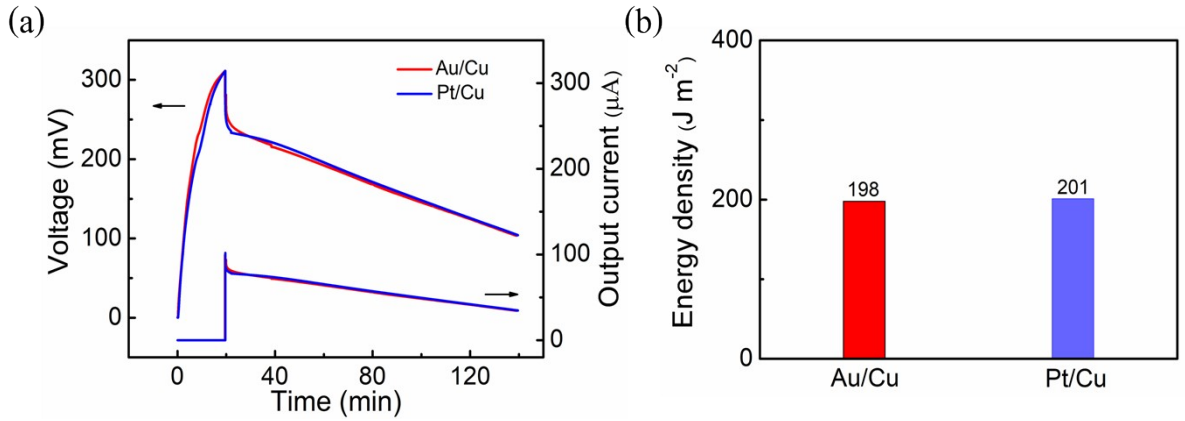

Figure S24. The comparison of a) measured voltage curves and b) output energy density in 2 h for the two as-fabricated i-TE cells: Au/Cu | Gelatin/0.8 mM GTA-KCl-$FeCN^{4-/3-}$ (r_v = 2.8) | Au/Cu and Pt/Cu | Gelatin/0.8 mM GTA-KCl-$FeCN^{4-/3-}$ (r_v = 2.8) | Pt/Cu at ΔT = 23 K (temperature range: from 21 °C to 44 °C).

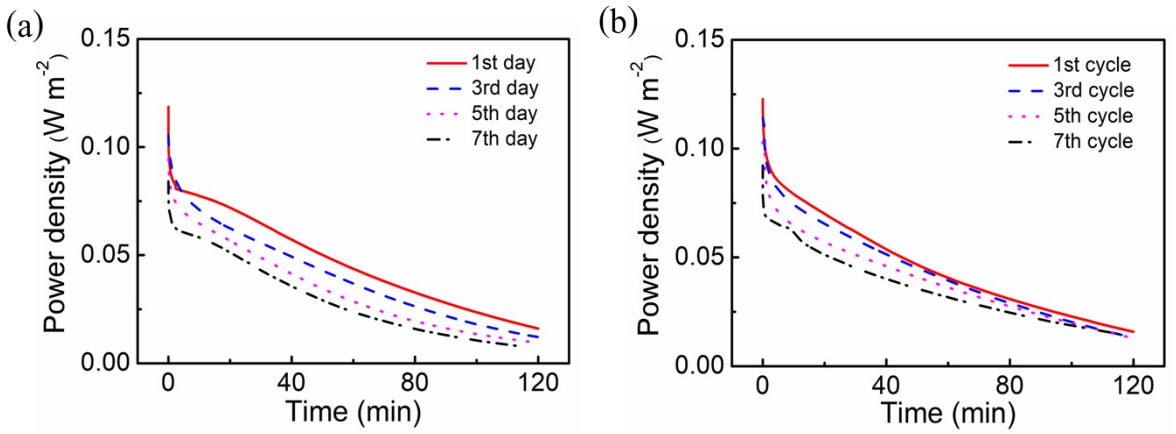

Figure S25. The comparison of power output density for 2 h on the first, second, third, and fourth day (cycle) using two long-time cyclic working modes. a) Working-rest mode. b) Continuous-working mode.

References

[1] C. G. Han, X. Qian, Q. Li, B. Deng, Y. Zhu, Z. Han, W. Zhang, W. Wang, S. P. Feng, G. Chen and W. S. Liu, *Science*, 2020, **368**, 1091-1098.

[2] Y. Liu, S. Zhang, Y. Zhou, M. A. Buckingham, L. Aldous, P. C. Sherrell, G. G. Wallace, G. Ryder, S. Faisal, D. L. Officer, S. Beirne and J. Chen, *Adv. Energy Mater.*, 2020, **10**, 2002539.

[3] Z. Lei, W. Gao, W. Zhu and P. Wu, *Adv. Funct. Mater.*, 2022, **32**, 2201021.

[4] Z. Lei, W. Gao and P. Wu, *Joule.*, 2021, **5**, 2211-2222.

[5] D. Zhang, Y. Mao, F. Ye, Q. Li, P. Bai, W. He and R. Ma, *Energy Environ. Sci.*, 2022, **15**, 2974-2982.

[6] Y. C. Li, Q. Li, X. Zhang, B. Deng, C. Han and W. S. Liu, *Adv. Energy Mater.*, 2022, **12**, 2103666.

[7] T. J. Kang, S. Fang, M. E. Kozlov, C. S. Haines, N. Li, Y. H. Kim, Y. Chen and R. H. Baughman, *Adv. Funct. Mater.*, 2012, **22**, 477-489.

[8] D. Zhao, H. Wang, Z. U. Khan, J. C. Chen, R. Gabrielsson, M. P. Jonsson, M. Berggren and X. Crispin, *Energy Environ. Sci.*, 2016, **9**, 1450-1457.

[9] S. L. Kim, H. T. Lin and C. Yu, Thermally Chargeable Solid-State Supercapacitor. *Adv. Energy Mater.* 2016, **6**, 1600546.

[10] Z. A. Akbar, J.-W. Jeon and S.-Y. Jang, *Energy Environ. Sci.*, 2020, **13**, 2915-2923.